Vol. 29 • No. 5 • February 2 • 2017

www.advmat.de

ADVANCED MATERIALS

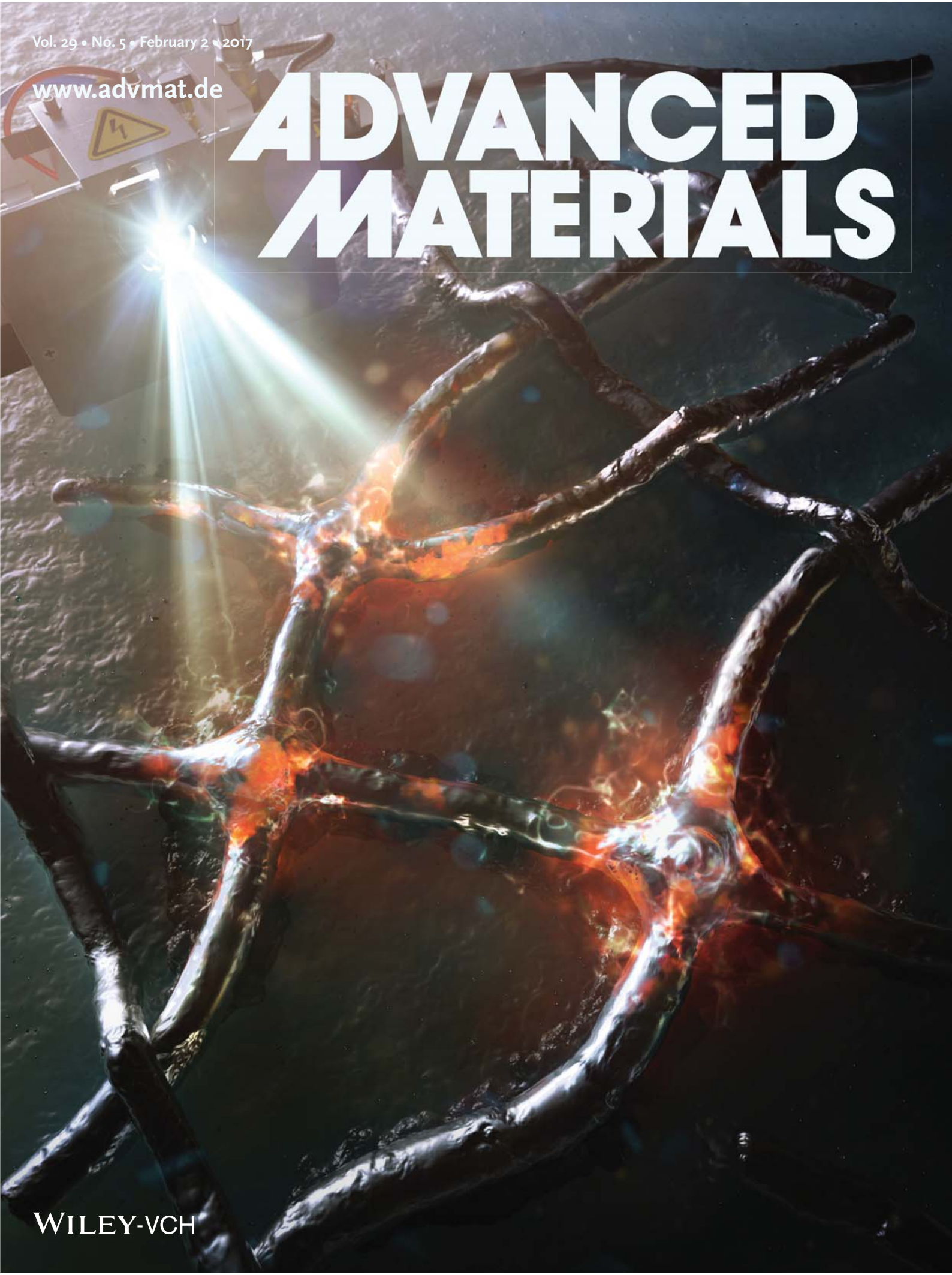

WILEY-VCH

ADVANCED MATERIALS
www.advmat.de

ADVANCED SCIENCE NEWS
www.advancedsciencenews.com

Flash-Induced Self-Limited Plasmonic Welding of Silver Nanowire Network for Transparent Flexible Energy Harvester

*Jung Hwan Park, Geon-Tae Hwang, Shinho Kim, Jeongmin Seo, Hong-Jin Park, Kyoungsik Yu, Taek-Soo Kim, and Keon Jae Lee**

With rapid advancement in the field of transparent and flexible electronics, we are on the verge of an enormous breakthrough in wide ranging fields from individual human healthcare to social networking.[1–7] For example, transparent flexible displays can be applied to augmented reality (AR) and the internet of things (IoTs), enabling 3D, intuitive, and bilateral communication based on experiential learning interface and user-customized information.[8] The fields where transparent flexible devices are used can be expanded to various energy applications such as energy harvesters,[9,10] batteries,[11] and supercapacitors[12,13] on plastics and realize aesthetically pleasing, sustainable, and maintenance-free, self-powered electronic systems.

Flexible transparent conducting electrodes (FTCEs, an essential element of flexible optoelectronics) such as graphene,[14–17] carbon nanotubes (CNTs),[18,19] and metallic nanowires (NWs)[20–24] have been extensively studied to replace indium tin oxide (ITO) due to its brittle ceramic nature and the scarcity of indium. However, carbon-based nanomaterials including graphene and CNTs exhibit high sheet resistance and low optical transparency owing to either low intrinsic carrier concentration or high tube–tube resistance.[25,26] Although bulk heating[27] and mechanical pressing[28,29] can improve the optoelectronic properties of metallic NW electrodes, they can damage the active device layer.

Recently, plasmonic interactions of nanomaterials that utilize various kinds of light sources including lasers (continuous wave (CW) or pulsed type) and arc lamps (CW arc or flash lamp) have received attention as a new technique for welding metal NWs.[30–35] Light-induced heating can generate extreme hot spots only at the NW junctions to achieve atomic mass transport between the neighboring materials for the formation of a fully welded metal NW network.[30] However, laser welding of a focused spot beam has a limitation with respect to mass production capability due to its time-consuming serial process compared to other large-area electronic processes.[36] The necessity of high optical power density (30 W cm^{-2}) of the CW arc lamp would also impede the commercial application of large scale FTCEs with inherent problems of huge power consumption and safety concerns.[37] From the perspective of a low-cost and broad spectrum light source, xenon flash lamps have attracted a great deal of attention due to their high output efficiency, fast processing, large-area processability, and compatibility with roll-to-roll manufacturing.[38–40] Despite the advantages of the flash-induced material process, industrially needed performance of NW networks (below 10 Ω sq^{-1} at transmittance of 90%)[25] based on theoretical photothermal investigations has not been reported, restricting the demonstration of current-driven applications due to significant power losses and resistive-capacitive delays.

Another critical issue of FTCEs is related to interfacial adhesion between electrodes and plastic substrates.[41,42] The delamination of conductors from polymer substrates can seriously deteriorate the overall reliability, functionality, and lifetime of flexible electronic devices.[43] A variety of techniques such as applying strong pressure,[28,29] in situ polymerization,[44] and encapsulation[20] have been addressed to improve the adhesion of FTCEs. Unfortunately, previously reported FTCEs do not satisfy industrial standards of adhesion properties including fragility, scratch resistance, endurance, and performance degradation, which should be accompanied by a quantitative analysis of the adhesion energy.

Herein, we report the flash-induced plasmonic interactions of silver nanowires (AgNWs) for exceptionally low sheet resistance (≈5 Ω sq^{-1}), high transparency (90%), and strong adhesion on plastic substrates. Localized heat energy with a self-limited photothermal reaction could be generated at the junctions of NWs, resulting in ultrafast and completely welded AgNWs. In addition, the spectral peaks in the near-infrared (NIR) region could locally melt the interface between the AgNW network and a polyethylene terephthalate (PET) substrate by surface plasmon polaritons (SPPs), and 310% higher adhesion force of AgNWs to the PET than that of pristine AgNW/PET film was demonstrated. To investigate the photothermal effect on surface

J. H. Park, Dr. G.-T. Hwang, Prof. K. J. Lee
Department of Materials Science and Engineering
Korea Advanced Institute of Science and Technology (KAIST)
291 Daehak-ro, Yuseong-gu, Daejeon 305-701, Republic of Korea
E-mail: keonlee@kaist.ac.kr
S. Kim, Prof. K. Yu
Department of Electrical Engineering
Korea Advanced Institute of Science and Technology (KAIST)
291 Daehak-ro, Yuseong-gu
Daejeon 305-701, Republic of Korea
J. Seo, Prof. T.-S. Kim
Department of Mechanical Engineering
Korea Advanced Institute of Science and Technology (KAIST)
291 Daehak-ro, Yuseong-gu, Daejeon 305-701, Republic of Korea
Dr. H.-J. Park
BSP Co., Ltd.
126 Beolmal-ro, Dongan-gu, Anyang
Gyeonggi-do 14057, Republic of Korea

DOI: 10.1002/adma.201603473

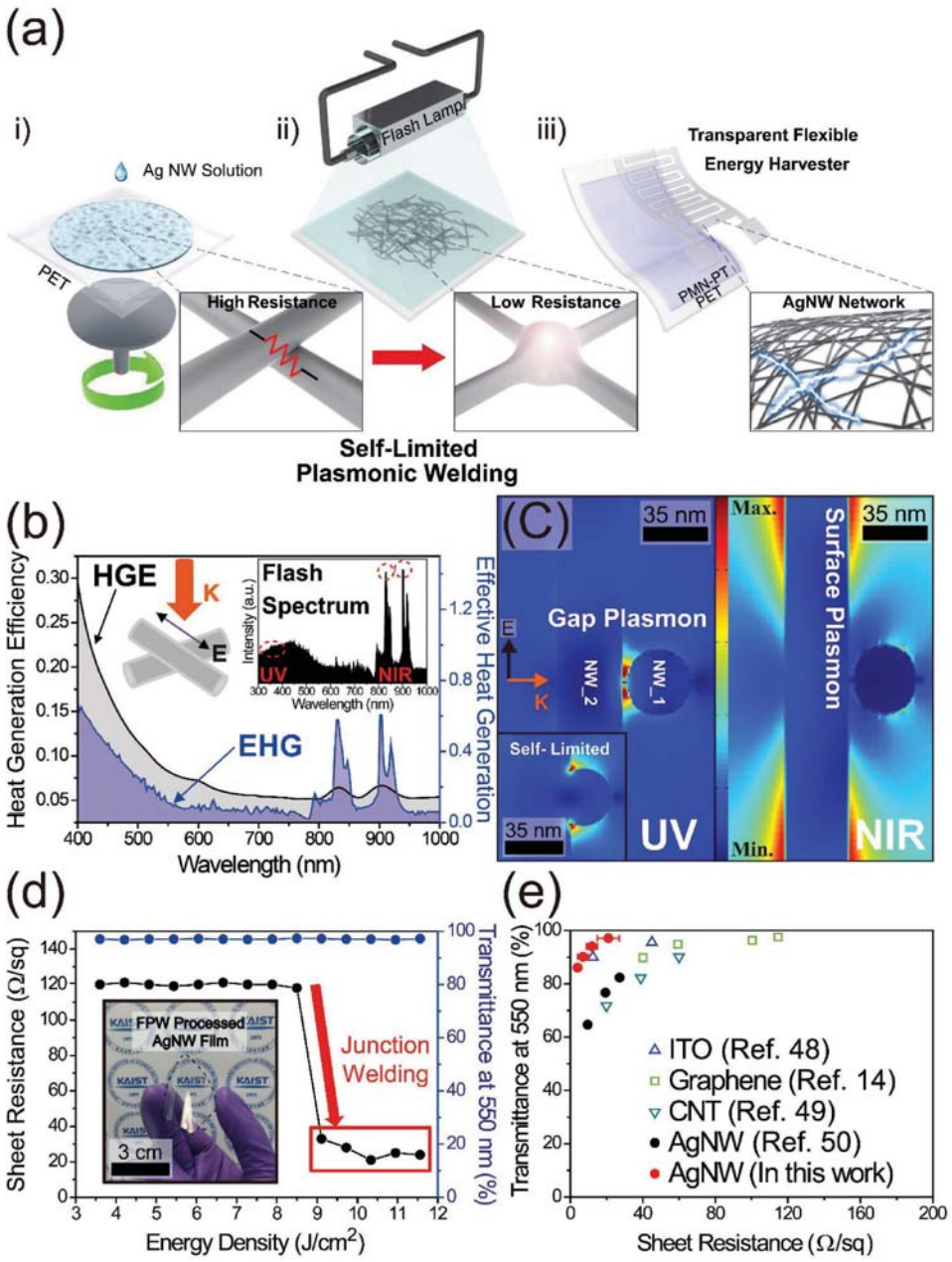

Figure 1. a) Schematic illustration of the AgNW FPW procedure and conceptual application towards a transparent flexible energy harvester. b) The FDTD simulation results of HGE and EHG for light polarized parallel to the first NW. The inset shows the spectrum of the xenon flash lamp. c) The local field distribution at a NW junction. The field enhancement response under the UV spectrum (400 nm) at the NW gap (left image). The inset shows FDTD simulation results that exhibit the self-limiting nature of the FPW. The field distribution caused by SPP (right image) under 800 nm electromagnetic wavelength. d) The sheet resistance of AgNW transparent conductor subject to different energy density of the flash lamp. The inset shows a photographic image of the AgNW/PET film after the FPW process. e) Plot of transmittance versus sheet resistance at 550 nm wavelength for films of FPW-treated AgNWs, with AgNWs, CNTs, graphene, and ITO as references.

adhesion, we performed quantitative DCB peel test measurements of the FTCE fracture force. The mechanism underlying effective welding and adhesion strengthening for the AgNW network was theoretically investigated by a 3D finite-difference time-domain (FDTD) analysis. Finally, the flash-activated AgNWs were utilized as a transparent electrode of a flexible piezoelectric energy harvester with a $Pb(Mg_{1/3}Nb_{2/3})O_3$–$PbTiO_3$ (PMN–PT) single crystal thin film. Despite the harsh voltage poling process and bending fatigue test, the transparent flexible energy harvester shows outstanding transmittance of ≈80% as well as high output performance of 38 V output voltage and 6.8 μA cm^{-2} current density, respectively.

Figure 1a schematically illustrates the procedure for flash-induced plasmonic welding (FPW) of AgNWs and its conceptual application to a transparent flexible energy harvester. The detailed process is as follows: (i) AgNW Ink (Nanopyxis) was

spin-coated onto a precleaned PET film to form a AgNW network with high junction resistance; (ii) the AgNW film was exposed to xenon flash light (pulse duration of 660 μs) with optimized energy; and lastly, (iii) a fully transparent flexible energy harvester was demonstrated using flash-induced plasmonic-welded AgNWs. To provide the theoretical mechanism of the plasmonic effect of the flash-induced process, FDTD simulations were performed, as shown in Figure 1b,c. In the simulation, a plane wave (wavelength in 400–1000 nm) was illuminated to perpendicularly crossed AgNWs with 35 nm diameter an intergap spacing of 2 nm by polyvinylpyrrolidone (PVP). Figure 1b shows heat generation efficiency (HGE) and effective heat generation (EHG) by polarized light in parallel to the top AgNWs. The HGE was defined by the fraction of incident light energy that is converted to heat, whereas EHG was defined as the product of the HGE and normalized lamp spectrum. Interestingly, the high EHG peaks were observed in ultraviolet (UV, wavelength in 400 nm) and NIR (wavelength in 830 and 900 nm) frequencies, indicating that intensive thermal energy can be generated by the UV and NIR light. As shown in Figure 1c, the strong electric fields at the NW gap and surface were induced by UV and NIR electromagnetic waves, respectively, enabling efficient light-driven heating. A concentrated gap field at UV could be generated by coupling the electromagnetically induced dipole moment of the AgNWs which can be expressed by Equation (1)[45]

$$E = E_0 \frac{\varepsilon_1 - \varepsilon}{\varepsilon_1 + \varepsilon} \frac{a^2}{\rho^2} \tag{1}$$

where E is the scattered electric field, E_0 is the electric field of the incident light, ε and ε_1 are the frequency-dependent permittivity of the air and AgNW, a is the NW radius, and ρ is the distance from the NW center. The gap plasmons can focus electromagnetic waves in an extremely limited space within the diffraction limit and then create localized hot spots at the junctions of AgNWs. This light-induced heat generation could be simulated by the joule Equation (2),[46] as shown in Figure S2 in the Supporting Information

$$q = \frac{\omega}{2} \mathrm{Im}(\varepsilon) |E_1|^2 \tag{2}$$

where q is the volumetric heat source density inside the NWs, ω is the angular frequency of the external field, and E_1 is the electric field in the AgNWs. As shown in Figure S3 in the Supporting Information, the heat generation could be enhanced for the larger diameter of AgNWs since the strength of the polarizability is increased. However, it deteriorates the optoelectronic properties of the NW network because of the low aspect ratio of the AgNWs.[47] The inset of Figure 1c and Figure S4 in the Supporting Information show that the HGE is significantly reduced as the gap distance is decreased and overlapped. When the NWs are physically welded together, the electromagnetic field in the NWs vanishes, and therefore the heat generation is also decreased, as shown in Figure S5 in the Supporting Information. This self-limiting nature can enhance material stability because it prevents the AgNW network from breaking up even under multiple flash irradiation. The right image of Figure 1c shows the SPP mode along the NW surface induced by the electromagnetic field of NIR spectral frequency. As the wavelength of the incident electric field increases to 800 nm NIR, the field at the metal dielectric interface was increased, as shown in Figure S6 in the Supporting Information, while the gap plasmons by UV (wavelength of 400 nm) gradually decreased. This electromagnetic field at the NW surface enables thermally induced modification of the PET surface, and thus strengthening adhesion of the AgNW film. Figures S7–S10 in the Supporting Information show the plasmonic responses of the AgNWs for the polarized light (400–1000 nm) perpendicular to the first NW, which exhibits similar results with NW reactions for polarized light (400–1000 nm) parallel to the top NW. To investigate the temperature generated in the NWs by photothermal interactions, we performed finite element method (FEM)-based thermal simulation with the PET to consider substrate effect. As shown in Figure S11 in the Supporting Information, we found that the temperature of the top AgNW could be increased over 300 °C, indicating that the junction welding effect could occur. The FPW effects on AgNW properties such as sheet resistance and transmittance were measured. The sheet resistance of the AgNW film dramatically decreased by 84.1%, from 120 to 19 Ω sq^{-1}, after flash light exposure at the optimized energy density of ≈10.3 J cm^{-2} with an extremely high transparency of 98% at 550 nm wavelength (Figure 1d). Additional performance enhancement in AgNW conductivity was not observed when the flash light with higher energy (over 10.3 J cm^{-2}) was irradiated on the AgNW network, indicating that the FPW process is well optimized in our flash system. To our best knowledge, this value is the highest optoelectronic property ever reported for light welded metal NWs. In contrast to time-consuming furnace heating, the ultrashort UV pulse of flash light facilitates rapid and localized junction annealing of the AgNW network. This outstanding performance compared to previous flash-induced works could be attributed to our well-designed flash lamp, composed of a compact and efficient parabolic reflector for low electromagnetic interference, as shown in Figure S12 in the Supporting Information. To compare the electrical and optical properties between this work and previous reports, experimental data were plotted as a function of the sheet resistance and transmittance for FPW-treated AgNWs, ITO,[48] and other transparent conductors such as graphene,[14] carbon nanotubes (CNTs),[49] and reference AgNWs[50] (Figure 1e). Our flash-induced plasmonic-welded AgNWs outperform ITO films and other previous transparent electrodes, showing excellent sheet resistance of ≈5 Ω sq^{-1} at a high transparency of ≈90%.

The FPW effect on the morphological evolution of the AgNW junctions was characterized by scanning electron microscopy (SEM) and transmission electron microscopy (TEM). **Figure 2**a and its inset show plane-view SEM images of welded and pristine AgNWs after and before FPW treatment, respectively. The plasmonic-welded junctions caused by flash-induced solidification of melted silver atoms can be observed in Figure 2a, whereas distinct nanowire junctions of pristine AgNWs are shown in the inset of Figure 2a. X-ray diffraction (XRD) results of the inset of Figure 2b reveal that the FPW-processed AgNWs were not oxidized during high temperature flash welding. In addition, the oxidation stability of the

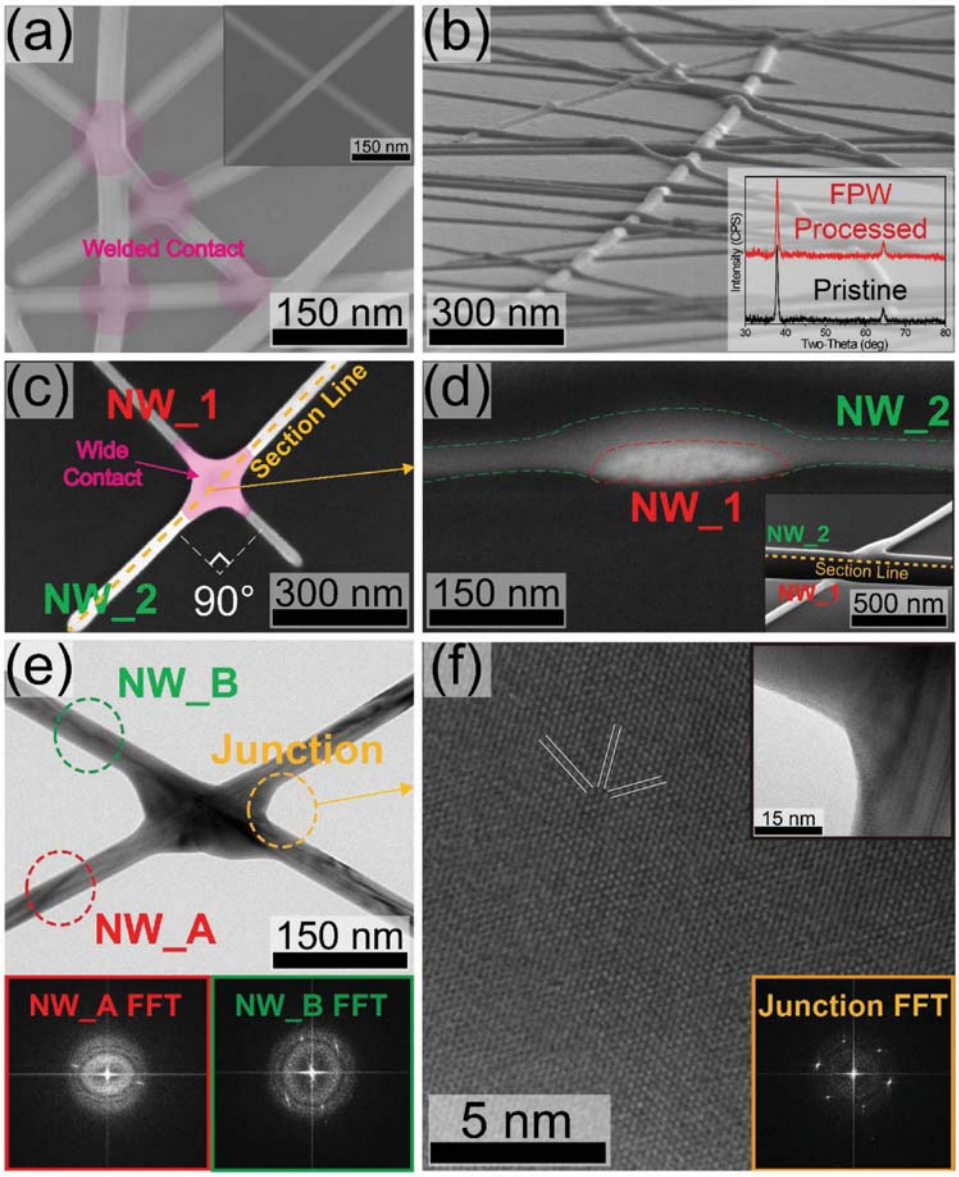

Figure 2. Morphological evolution of FPW-processed AgNWs on a PET substrate. a) A plane view SEM image of flash-induced plasmonic-welded AgNWs. The inset shows a distinct NW junction of pristine AgNWs. b) A tilted view SEM image of AgNWs after the FPW process. The inset shows the XRD spectrum of the FPW-treated AgNWs, which presents an oxidation-free AgNW network. c) A plane view HR-SEM image of welded AgNWs. d) A cross-sectional SEM image of a flash-induced plasmonic-welded AgNW junction enabled by the focused ion beam (FIB)-SEM process. e) A plane view TEM image of junction welded AgNWs. The inset presents the power spectrum from the FFT of each nanowire, which shows two distinct nanowires are merged together and welded. f) The lattice resolved TEM image of a welded junction of AgNWs in figure (e). The inset shows a TEM image and FFT pattern of a fused junction.

FPW-treated AgNW network has been investigated, as shown in Figures S13 and S14 in the Supporting Information, which presents high oxidation resistance of FPW-processed AgNWs under ambient environments. The tilted-view SEM image in Figure 2b and Figure S16 in the Supporting Information show conformal and fused nanocontacts between AgNWs even after multiple flash light radiation because of the self-limited process. The representative junction of welded AgNWs (marked by NW_1 and NW_2) with a crossing angle of 90° was further investigated by high-resolution SEM (HR-SEM), as presented in Figure 2c. The optically welded junction of AgNWs exhibits wide contact formation and dramatic improvement of the junction conductance. Figure 2d shows the cross-section morphology of a welded junction of AgNWs. The NW_1 and NW_2 of 35 nm diameter were fully fused with each other at the intersection without the formation of an inter-insulating layer. Detailed information on the cross-sectioning procedures of the AgNW junction can be found in Figure S17 in the Supporting Information. Figure 2e shows a high resolution TEM image of welded AgNWs (marked by NW_A and NW_B) and fast Fourier transform (FFT) patterns (red: NW_A, green: NW_B), respectively. The high resolution TEM image clearly shows that the

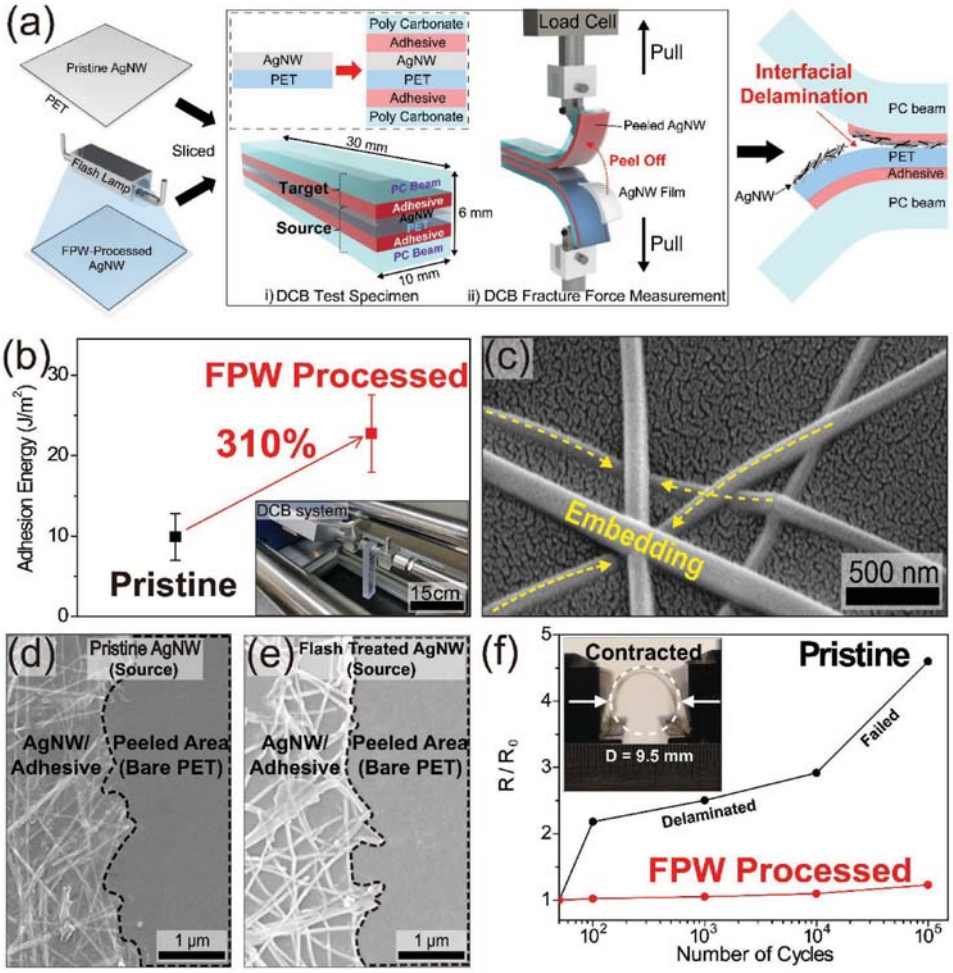

Figure 3. a) Schematic illustrations of the custom-designed DCB peel test. b) The adhesion energy measurement results of as-prepared and flash-treated AgNW film evaluated by quantitative DCB peel test. The inset shows a photographic image of the DCB peel test system. c) Morphological SEM image of the AgNWs embedded into the PET film. d) The top-view SEM image of the DCB specimen (source part) prepared by pristine AgNW/PET film after the peel test. e) The top-view SEM image of the DCB specimen (source part) prepared by flash-treated AgNW network after the peel test. f) The normalized resistance of pristine and FPW-treated AgNW films under a cyclic bending test. The bending radius was 4.75 mm and the frequency was 1 Hz, and the inset shows an optical image of the AgNW film in a bending state.

two AgNWs are merged and firmly welded together. The FFT patterns of the two NWs exhibited different directions, verifying that NW_A and NW_B are individually distinct from each other. As shown in Figure 2f and its inset, the magnified TEM image of a NW junction in Figure 2e (indicated as a yellow circle) and its FFT reveal that NW_A and NW_B are connected and coexist at the NW intersection by the FPW process.

Figure 3a shows a schematic illustration of the custom-designed double cantilever beam (DCB) peel test for quantitatively monitoring the FTCE fracture force of the flash-irradiated AgNW/PET film. Pristine and flash-treated AgNWs on PET substrates were sliced into 10 mm width and 30 mm length. An epoxy adhesive was deposited between the PET substrate and the polycarbonate (PC) beam (thickness of 3 mm), and cured at 80 °C for 30 min to prepare the DCB source specimen. In addition, the PC beam was additionally attached by adhesive on the AgNWs of the source specimen to complete the DCB sample. The adhesive thickness of each DCB specimen shows uniform thickness (1–2 μm), as shown in Figure S18 in the Supporting Information. Consistent 35 mm long precracks were introduced at the source/target interface of the DCB specimens by controlling the amount of epoxy adhesive and inducing initial fatigue crack growth for a quantitative comparison of the measured interfacial adhesion energy.[51] These DCB specimens were pulled by a linear actuator at a constant displacement rate of 0.1 mm s^{-1} for measuring the delamination force in J m^{-2}. The measured adhesion energy of the FPW-processed sample was 30.7 J m^{-2}, exhibiting 310% higher adhesion force than that of the pristine specimen (Figure 3b). This significant property of the critical adhesion parameter can improve the product lifetime,[52] which is attributed to NIR spectral irradiation of the flash lamp. The specific light could excite the SPP of AgNWs[53] and locally melt the PET surface, causing embedment of AgNWs into PET and enhancement of the adhesion (Figure 3c). To experimentally verify the local melting of PET by flash lamp, we removed the pristine and flash light

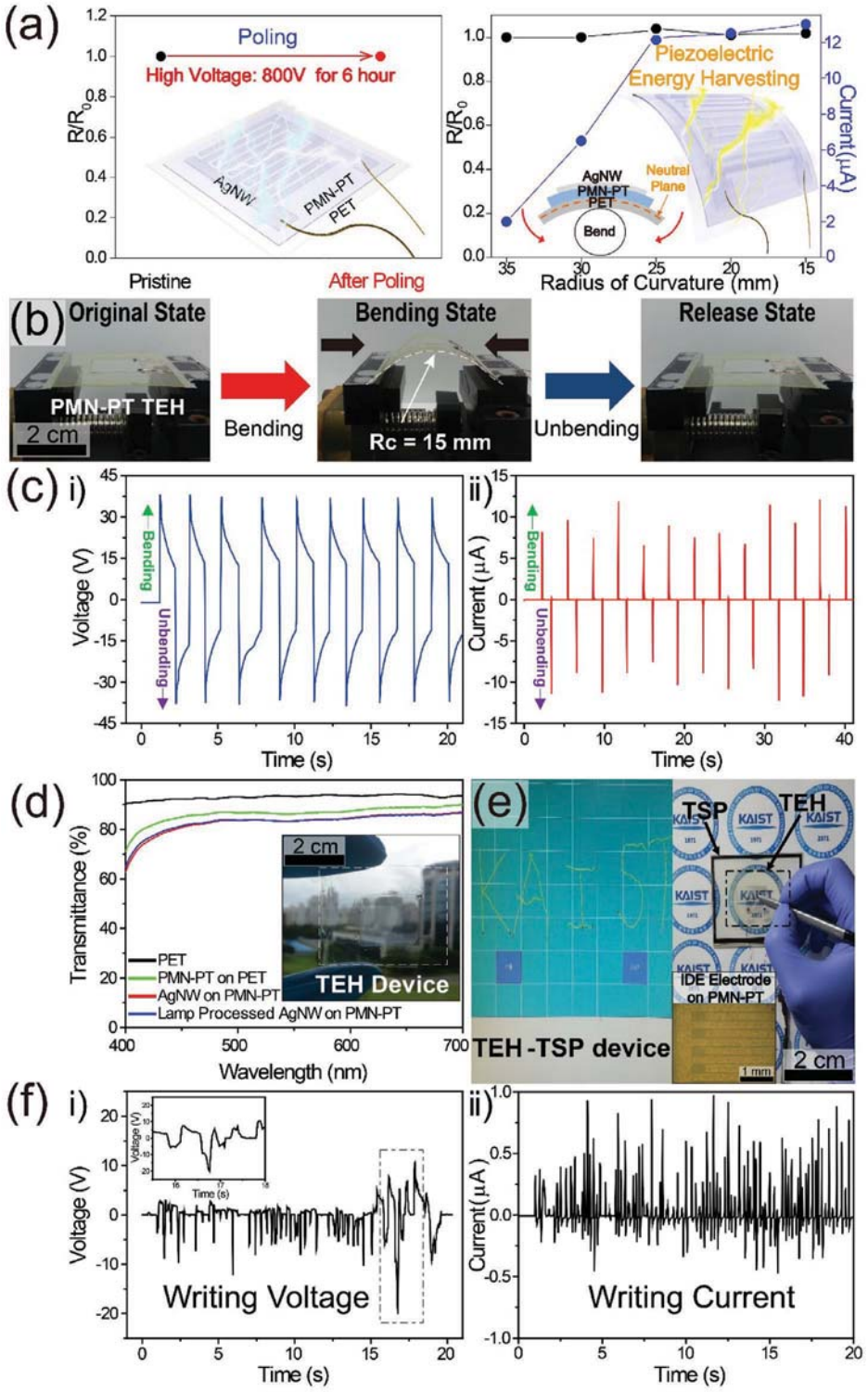

Figure 4. a) Stable performance of FPW-treated AgNWs and transparent energy harvester under poling process and bending stress. b) Optical images of the flexible transparent PMN–PT harvesting device in the original, bending, and release states for power generation. c) The open-circuit voltage (i) and short-circuit current signals (ii) generated from the energy harvester during periodical bending and unbending motions. d) The transmittance of PET, PMN–PT on PET substrate, and transparent energy harvesting device based on pristine AgNWs and FPW-treated AgNWs. The inset shows a photographic image of the transparent flexible energy harvesting device. e) Demonstration of the TSP energy harvesting system enabled by the PMN–PT thin film energy harvester and the FPW-processed AgNW conductor. The inset shows a microscopic image of interdigitated AgNW electrodes treated by the FPW method on PMN–PT film. f) The measured output voltage (i) and current peaks (ii) generated from the transparent flexible energy harvester with the writing touch of a pen. The inset (f–i) exhibits a magnified view of the black dotted region.

processed AgNWs on PET by etching the Ag to see the locally melted polymer surface. As shown in Figure S19a in the Supporting Information, the surface of the PET after etching the pristine AgNWs shows clear polymer surface without local melting region. However, we could find that the PET surface after removing the flash-treated AgNWs was melted along the AgNWs (reddish colored area) due to the heat generated through the excitation of the AgNW SPPs (Figure S19b, in the Supporting Information). Figure S20 in the Supporting Information shows the higher resolution SEM images of flash-irradiated AgNW/PET before and after Ag etching for further investigation. As shown in Figure S20b in the Supporting Information, we could see locally melted PET surface. In spite of intensive heat processing on thermally sensitive PET, the film deformation or other negative side effects on polymer properties were not observed. This low temperature process merit of flash-induced nanomaterial interactions will provide powerful strategies for realizing flexible/stretchable electronics by overcoming heat incapability on polymer substrates.[54,55] After the DCB peel test, the delaminated interface was analyzed to clarify the fracture mechanism of each sample. Figures 3d,e show top-view SEM images for the peeled specimens of as-prepared and FPW-processed AgNWs. The interfacial delamination of NWs was observed for both pristine and FPW-treated AgNWs, which shows that the adhesion energy of the AgNW/PET interface was precisely characterized. To prove the wavelength dependence of the NW–NW and NW–PET interaction, we set up the bandpass filter (Thorlabs, FGB 37S) to block the NIR spectrum (from 750 to 1000 nm wavelength) before flash lamp processing (Figure S22, Supporting Information). The sheet resistance of the AgNW film (transmittance of 98% at 550 nm wavelength) was decreased from 120 to 32 Ω sq^{-1} at the energy density of 10.3 J cm^{-2}, confirming the junction nanowelding effect, as shown in Figure S23 in the Supporting Information. The SEM analysis was additionally performed and it showed the firmly welded AgNW junctions (Figure S24 in the Supporting Information). On the other hand, Figure S25 in the Supporting Information showed that the adhesion enhancement effect was not occurring, which was based on DCB adhesion energy measurement results of pristine and flash lamp processed AgNW/PET film. The bending stability of flash-induced plasmonic-welded AgNWs was further evaluated by monitoring the normalized resistance dependence to the bending radius, down to 4.75 mm, with repeated bending/unbending motions at a frequency of 1 Hz, as shown in Figure 3f. The normalized resistance of the as-prepared AgNWs increased dramatically to 2.2 within 100 bending cycles and eventually rose to 4.6 at 100 000 cycles. On the other hand, the normalized resistance of the FPW-treated AgNWs exhibited little change even after 100 000 bending cycles. This outstanding reliability under the bending fatigue test was ascribed to the interlocking structure of the AgNW/PET interface by NW embedment, inhibiting the delamination of AgNWs under bending.

To demonstrate the practical uses of flash-induced plasmonic-welded AgNWs, we fabricated a transparent and flexible single crystalline PMN–PT energy harvester by integrating the FPW-treated AgNW electrodes into an actual flexible device.[56–60] In spite of the harsh poling process under a high voltage of 800 V for 6 h and tensile stress from bending motion, no performance degradation of the AgNWs and the piezoelectric harvester was observed, showing that FPW can be universally utilized for device fabrication (**Figure 4**a). Figure 4c-i,ii shows the measurement results of the transparent flexible energy harvester during the repeated bending/unbending motions, where the open-circuit voltage and short-circuit current values were 38 V and 12.5 μA. The output current density of the flexible PMN–PT energy harvester (activated electrode area: 1.3 cm × 1.41 cm) was calculated as 6.8 μA cm^{-2}; this value is higher than the current density of a previous transparent piezoelectric harvester.[61] Furthermore, the flexible energy harvester presented high transmittance of ≈80% at a wavelength of 550 nm, which is enabled by the excellent optoelectronic performance of the flash lamp annealed AgNW electrodes (Figure 4d). This transparency value is remarkable compared to previously reported transparent and flexible piezoelectric energy harvesters using ITO and graphene as electrode layers.[59,61] Our transparent and flexible energy device consequently achieved not only high electric output performance but also outstanding optical transparency. In addition, we demonstrated a touch screen panel (TSP) energy harvesting system that can generate electric energy by writing on the TSP (Figure 4e). When the top surface of the TSP energy harvester was pushed by the writing motion of a pen, a randomly deformed energy harvester generated oscillating output voltage of 20 V and output current of 1 μA (Figure 4f-i,ii).

In summary, we have presented FPW-induced transparent and flexible AgNW electrode with excellent sheet resistance, high transparency, and strong adhesion. The broad UV radiation of a flash lamp enabled local junction heating and fully welded AgNWs with a sheet resistance of 5 Ω sq^{-1} at a transmittance of ≈90 %. Simultaneously, the intensive SPP generated by NIR could thermally modify the PET surface and enhance the adhesion property of AgNWs. A delamination fracture force of 30.7 J m^{-2} was measured for the FPW-treated specimen by custom-designed DCB peel test, exhibiting 310% higher peel strength compared to that of pristine AgNWs. The strong adhesion on the plastic substrate provides a significant enhancement of the bending stability over 100 000 cycles at a curvature radius of 4.75 mm. The 3D FDTD investigations theoretically confirmed that junction welding and adhesion strengthening of the AgNW network could be incited by UV and NIR light, respectively. The flash-induced plasmonic-welded AgNWs were employed for a transparent flexible PMN–PT energy harvester. Despite a harsh poling process and bending stress, the transparent piezoelectric harvesting device shows an excellent output voltage of 38 V and a current density of 6.8 μA cm^{-2} with an outstanding transparency of ≈80%. Finally, a TSP energy harvesting system was demonstrated, and it could generate output voltage of 20 V and output current of 1 μA by pen writing. A flash-induced process with a theoretical plasmonic understanding can provide an important tool for transparent electrodes of metal NWs that can be used in various next-generation flexible optoelectronics such as displays and biomedical applications.

Experimental Section

Optical Simulation: The 3D FDTD provided by Lumerical Solutions Inc. was employed to characterize optical properties of crossed AgNWs.

In this simulation, plane wave (from 400 to 1000 nm wavelength) was illuminated to perpendicularly crossed AgNWs with the 35 nm diameter which is same size of synthesized NWs. As an evaluation for the PVP spacing, the two AgNWs were separated with 2 nm gap. To eliminate fictious resonance resulting from finite NW length, a perfectly matched layer was used to boundary condition. The plasmonic responses of AgNWs for two orthogonally polarized light were analyzed because the unpolarized electromagnetic wave can be represented as the sum of two perpendicularly polarized light. The optical constants of Ag from Palik were employed for the simulation.

Bending Test: Pristine and FPW-processed AgNWs on a PET substrate were cut into 12 mm width and 25 mm length for bending test specimens and both edges of the sample were firmly fixed to the bending machine for the fatigue test. The cyclic bending test was performed by using a custom-designed bending machine (QS48, TPC motion). Electrical resistance was measured after each fatigue cycle step from 100 to 100 000 cycles with a frequency of 1 Hz.

Fabrication of Transparent and Flexible Energy Harvester: A (001)-oriented 0.72 PMN–0.28 PT single crystal film on a PET substrate was prepared, as described in our previous study.[57] Briefly, the PMN–PT single crystal film was exfoliated from the bulk substrate by using tensile stress of the deposited Ni film. The optical adhesive (Norland Products) was employed to bond the freestanding piezoelectric layer to a PET substrate (110 μm), and the Ni etchant (Transene, TFG) was used to wet-etch the top Ni film. A photoresist (AZ 5214) was spin-coated onto the PMN–PT film and negatively developed in the form of lateral-type interdigitated electrodes (IDEs); the IDEs had an electrode width of 100 μm, an intergap of 100 μm, and 36 finger pairs. The AgNW ink was spin-coated onto the prepatterned photoresist and dried for 30 s in ambient conditions. The AgNW film was patterned by a lift-off process and annealed by the FPW method. To protect the device, SU-8 (Microchem) was optionally coated on the transparent flexible energy harvester.

Measurement of Output Performance: The electric output performance of the transparent harvester during repeated bending/unbending motions for a strain of 0.3% on a plastic substrate, a strain rate of 2.2% s^{-1}, and a frequency of 0.25 Hz was characterized by a linear bending machine and a source meter in a faraday cage.

Demonstration of TSP Energy Harvesting System: The commercialized TSP (4-wire resistive type) was purchased from KOAT Solution. The TSP was connected to a computer by a flexible printed circuit board and operated by software (Touch Side) provided by KOAT Solution. The transparent flexible harvesting device was conformally integrated by using 3M adhesive to the TSP for demonstration of the TSP energy harvesting system. The energy harvesting and writing could be simultaneously accomplished by pen touching on the self-powered transparent device.

Characterizations: The morphological images were observed using an optical microscope (VHX-1000E, Keyence), SEM (Magellan 400, FEI company), FIB-SEM (Helios Nanolab 450 F1, FEI company), and TEM (Tecnai TF 30 ST, FEI company). The elemental and chemical compositions of pristine AgNWs and flash-induced plasmonic-welded AgNWs were monitored by using XRD (D/MAX-2500, Rigaku). The transmittance of an as-prepared AgNW network, FPW-processed AgNW film, and transparent flexible energy harvester was characterized by a UV–Visible spectrometer (Evolution 220, Thermo Fisher Scientific).

Supporting Information

Supporting Information is available from the Wiley Online Library or from the author.

Acknowledgements

J.H.P. and G.T.H. contributed equally to this work. This research was supported by Creative Materials Discovery Program through the National Research Foundation of Korea (NRF) funded by the Ministry of Science, ICT and Future Planning (grant code: NRF-2016M3D1A1900035), and the NRF Grant funded by the Korean Government (MSIP) (grant code: NRF-2016R1A5A1009926), as well as the Nano Material Technology Development Program through the NRF funded by the Ministry of Science, ICT and Future Planning (grant code: NRF-2016M3A7B4905609) and BSP corporation.

Received: July 1, 2016
Revised: October 8, 2016
Published online: November 28, 2016

[1] C. Keplinger, J. Y. Sun, C. C. Foo, P. Rothemund, G. M. Whitesides, Z. Suo, *Science* **2013**, *341*, 984.
[2] J. F. Wager, *Science* **2003**, *300*, 1245.
[3] X. Yu, T. J. Marks, A. Facchetti, *Nat. Mater.* **2016**, *15*, 383.
[4] S. Ju, A. Facchetti, Y. Xuan, J. Liu, F. Ishikawa, P. Ye, C. Zhou, T. J. Marks, D. B. Janes, *Nat. Nanotechnol.* **2007**, *2*, 378.
[5] H. Lee, Y. Lee, C. Song, H. R. Cho, R. Ghaffari, T. K. Choi, K. H. Kim, Y. B. Lee, D. Ling, H. Lee, S. J. Yu, S. H. Choi, T. Hyeon, D. H. Kim, *Nat. Commun.* **2015**, *6*, 10059.
[6] F. Fu, T. Feurer, T. Jager, E. Avancini, B. Bissig, S. Yoon, S. Buecheler, A. N. Tiwari, *Nat. Commun.* **2015**, *6*, 9932.
[7] C. W. Hsu, B. Zhen, W. Qiu, O. Shapira, B. G. DeLacy, J. D. Joannopoulos, M. Soljacic, *Nat. Commun.* **2014**, *5*, 4152.
[8] K. Austen, *Nature* **2015**, *525*, 22.
[9] F. R. Fan, L. Lin, G. Zhu, W. Wu, R. Zhang, Z. L. Wang, *Nano Lett.* **2012**, *12*, 3109.
[10] H. K. Park, K. Y. Lee, J. S. Seo, J. A. Jeong, H. K. Kim, D. Choi, S. W. Kim, *Adv. Funct. Mater.* **2011**, *21*, 1187.
[11] Y. Yang, S. Jeong, L. Hu, H. Wu, S. W. Lee, Y. Cui, *Proc. Natl. Acad. Sci. USA* **2011**, *108*, 13013.
[12] H. Y. Jung, M. B. Karimi, M. G. Hahm, P. M. Ajayan, Y. J. Jung, *Sci. Rep.* **2012**, *2*, 773.
[13] T. Chen, H. Peng, M. Durstock, L. Dai, *Sci. Rep.* **2014**, *4*, 3612.
[14] S. Bae, H. Kim, Y. Lee, X. Xu, J. S. Park, Y. Zheng, J. Balakrishnan, T. Lei, H. R. Kim, Y. I. Song, Y. J. Kim, K. S. Kim, B. Ozyilmaz, J. H. Ahn, B. H. Hong, S. Iijima, *Nat. Nanotechnol.* **2010**, *5*, 574.
[15] S. Pang, Y. Hernandez, X. Feng, K. Mullen, *Adv. Mater.* **2011**, *23*, 2779.
[16] X. Li, Y. Zhu, W. Cai, M. Borysiak, B. Han, D. Chen, R. D. Piner, L. Colombo, R. S. Ruoff, *Nano Lett.* **2009**, *9*, 4359.
[17] J. Wu, M. Agrawal, H. A. Becerril, Z. Bao, Z. Liu, Y. Chen, P. Peumans, *ACS Nano* **2010**, *4*, 43.
[18] Z. Wu, Z. Chen, X. Du, J. M. Logan, J. Sippel, M. Nikolou, K. Kamaras, J. R. Reynolds, D. B. Tanner, A. F. Hebard, A. G. Rinzler, *Science* **2004**, *305*, 1273.
[19] R. C. Tenent, T. M. Barnes, J. D. Bergeson, A. J. Ferguson, B. To, L. M. Gedvilas, M. J. Heben, J. L. Blackburn, *Adv. Mater.* **2009**, *21*, 3210.
[20] L. Hu, H. S. Kim, J. Y. Lee, P. Peumans, Y. Cui, *ACS Nano* **2010**, *4*, 2955.
[21] S. De, T. M. Higgins, P. E. Lyons, E. M. Doherty, P. N. Nirmalraj, W. J. Blau, J. J. Boland, J. N. Coleman, *ACS Nano* **2009**, *3*, 1767.
[22] A. R. Rathmell, S. M. Bergin, Y. L. Hua, Z. Y. Li, B. J. Wiley, *Adv. Mater.* **2010**, *22*, 3558.
[23] S. Hong, H. Lee, J. Lee, J. Kwon, S. Han, Y. D. Suh, H. Cho, J. Shin, J. Yeo, S. H. Ko, *Adv. Mater.* **2015**, *27*, 4744.
[24] H. Lee, S. Hong, J. Lee, Y. D. Suh, J. Kwon, H. Moon, H. Kim, J. Yeo, S. H. Ko, *ACS Appl. Mater. Inter.* **2016**, *8*, 15449.
[25] T. Gao, Z. Li, P. S. Huang, G. J. Shenoy, D. Parobek, S. Tan, J. K. Lee, H. Liu, P. W. Lee, *ACS Nano* **2015**, *9*, 5440.
[26] R. V. Salvatierra, C. E. Cava, L. S. Roman, A. J. G. Zarbin, *Adv. Funct. Mater.* **2013**, *23*, 1490.

[27] J. Y. Lee, S. T. Connor, Y. Cui, P. Peumans, *Nano Lett.* **2008**, *8*, 689.
[28] W. Gaynor, G. F. Burkhard, M. D. McGehee, P. Peumans, *Adv. Mater.* **2011**, *23*, 2905.
[29] W. Gaynor, J. Y. Lee, P. Peumans, *ACS Nano* **2010**, *4*, 30.
[30] E. C. Garnett, W. Cai, J. J. Cha, F. Mahmood, S. T. Connor, M. G. Christoforo, Y. Cui, M. D. McGehee, M. L. Brongersma, *Nat. Mater.* **2012**, *11*, 241.
[31] S. Han, S. Hong, J. Ham, J. Yeo, J. Lee, B. Kang, P. Lee, J. Kwon, S. S. Lee, M. Y. Yang, S. H. Ko, *Adv. Mater.* **2014**, *26*, 5808.
[32] J. A. Spechler, C. B. Arnold, *Appl. Phys. A* **2012**, *108*, 25.
[33] J. Jiu, M. Nogi, T. Sugahara, T. Tokuno, T. Araki, N. Komoda, K. Suganuma, H. Uchida, K. Shinozaki, *J. Mater. Chem.* **2012**, *22*, 23561.
[34] P. Lee, J. Lee, H. Lee, J. Yeo, S. Hong, K. H. Nam, D. Lee, S. S. Lee, S. H. Ko, *Adv. Mater.* **2012**, *24*, 3326.
[35] J. Lee, P. Lee, H. Lee, D. Lee, S. S. Lee, S. H. Ko, *Nanoscale* **2012**, *4*, 6408.
[36] M. Takai, D. Bollmann, K. Haberger, *Appl. Phys. Lett.* **1994**, *64*, 2560.
[37] H. Lu, D. Zhang, X. Ren, J. Liu, W. C. H. Choy, *ACS Nano* **2014**, *8*, 10980.
[38] J. Perelaer, R. Abbel, S. Wunscher, R. Jani, T. V. Lammeren, U. S. Schubert, *Adv. Mater.* **2012**, *24*, 2620.
[39] D. Angmo, T. T. L. Olsen, M. Jorgensen, R. R. Sondergaard, F. C. Krebs, *Adv. Energy. Mater.* **2013**, *3*, 172.
[40] M. Csele, *Fundamentals of Light Sources and Lasers*, Wiley-VCH, Weinheim, Germany **2004**.
[41] R. Zhu, C. H. Chung, K. C. Cha, W. Yang, Y. B. Zheng, H. Zhou, T. B. Song, C. C. Chen, P. S. Weiss, G. Li, Y. Yang, *ACS Nano* **2011**, *5*, 9877.
[42] A. B. V. K. Kumar, C. W. Bae, L. Piao, S. H. Kim, *Mater. Res. Bull.* **2013**, *48*, 2944.
[43] B. Son, M. H. Ryou, J. Choi, T. Lee, H. K. Yu, J. H. Kim, Y. M. Lee, *ACS Appl. Mater. Inter.* **2014**, *6*, 526.
[44] X. Y. Zeng, Q. K. Zhang, R. M. Yu, C. Z. Lu, *Adv. Mater.* **2010**, *22*, 4484.
[45] H. J. Eom, *Electromagnetic Wave Theory for Boundary-Value Problems*, Springer, Berlin **2004**.
[46] L. D. Landau, E. M. Lifshitz, L. P. Pitaevski , *Electrodynamics of Continuous Media*, Pergamon, New York **1984**.
[47] R. M. Mutiso, M. C. Sherrott, A. R. Rathmell, B. J. Wiley, K. I. Winey, *ACS Nano* **2013**, *7*, 7654.
[48] A. R. Rathmell, B. J. Wiley, *Adv. Mater.* **2011**, *23*, 4798.
[49] A. Saha, C. Jiang, A. A. Marti, *Carbon* **2014**, *79*, 1.
[50] B. Deng, P. C. Hsu, G. Chen, B. N. Chandrashekar, L. Liao, Z. Ayitimuda, J. Wu, Y. Guo, L. Lin, Y. Zhou, M. Aisijiang, Q. Xie, Y. Cui, Z. Liu, H. Peng, *Nano Lett.* **2015**, *15*, 4206.
[51] R. H. Dauskardt, M. Lane, Q. Ma, N. Krishna, *Eng. Fract. Mech.* **1998**, *61*, 141.
[52] I. Lee, S. Kim, J. Yun, I. Park, T. S. Kim, *Nanotechnology* **2012**, *23*, 485704.
[53] J. V. D. Groep, P. Spinelli, A. Polman, *Nano Lett.* **2012**, *12*, 3138.
[54] S. Hong, J. Yeo, G. Kim, D. Kim, H. Lee, J. Kwon, H. Lee, P. Lee, S. H. Ko, *ACS Nano* **2013**, *7*, 5024.
[55] J. H. Park, S. Jeong, E. J. Lee, S. S. Lee, J. Y. Seok, M. Yang, Y. Choi, B. Kang, *Chem. Mater.* **2016**, *28*, 4151.
[56] G. T. Hwang, Y. Kim, J. H. Lee, S. Oh, C. K. Jeong, D. Y. Park, J. Ryu, H. Kwon, S. G. Lee, B. Joung, D. Kim, K. J. Lee, *Energy Environ. Sci.* **2015**, *8*, 2677.
[57] G. T. Hwang, H. Park, J. H. Lee, S. Oh, K. I. Park, M. Byun, H. Park, G. Ahn, C. K. Jeong, K. No, H. Kwon, S. G. Lee, B. Joung, K. J. Lee, *Adv. Mater.* **2014**, *26*, 4880.
[58] D. Choi, M. Y. Choi, W. M. Choi, H. J. Shin, H. K. Park, J. S. Seo, J. Park, S. M. Yoon, S. J. Chae, Y. H. Lee, S. W. Kim, J. Y. Choi, S. Y. Lee, J. M. Kim, *Adv. Mater.* **2010**, *22*, 2187.
[59] L. Lin, Y. Hu, C. Xu, Y. Zhang, R. Zhang, X. Wen, Z. L. Wang, *Nano Energy* **2013**, *2*, 75.
[60] Z. H. Lin, Y. Yang, J. M. Wu, Y. Liu, F. Zhang, Z. L. Wang, *J. Phys. Chem. Lett.* **2012**, *3*, 3599.
[61] J. Kwon, W. Seung, B. K. Sharma, S. W. Kim, J. H. Ahn, *Energy Environ. Sci.* **2012**, *5*, 8970.